Final Report (NCSU-SC0011631)
Superconducting Joints Between (RE)$Ba_2Cu_3O_{7-x}$ Coated Conductors via Electric Field Assisted Processing
DE-SC0011631, North Carolina State University
Principal Investigator: Professor Justin Schwartz, Justin_Schwartz@ncsu.edu, 919-515-0493
Covering the period May 1, 2014-March 31, 2017

I. Task and Timeline Summary

Here we report the results from a project aimed at developing a fully superconducting joint between two REBCO coated conductors using electric field processing (EFP). Due to a reduction in the budget and time period of this contract, we reduced the project scope and focused first on the key scientific issues for forming a strong bond between conductors, and subsequently focused on improving through-the-joint transport. A modified timeline and task list is shown in Table 1, summarizing accomplishments to date. In the first period, we accomplished initial surface characterization as well as rounds of EFP experiments to begin to understand processing parameters which produce well-bonded tapes. In the second phase, we explored the effects of two fundamental EFP parameters, voltage and pressure, and the limitations they place on the process. In the third phase, we achieved superconducting joints and established base characteristics of both the bonding process and the types of tapes best suited to this process. Finally, we investigated some of the parameters related to kinetics which appeared inhibit joint quality and performance.

Overall, significant progress was made towards our initial goal. A superconducting joint was developed, and the impact of many of the parameters which affect the bonding process were investigated and in some cases established. Currently, our best producible joints lack the current-carrying capacity to be used at an industrial level, but this is an area which can be addressed by some simple remedies, including simply bonding the conductors over a larger contacted area. In addition, although the films do suffer some T_c depression during bonding, the retained T_c remains well above the operating temperature of many magnets, even without post-annealing.

Table 1: Modified Project Tasks and Timeline

Task	Year 1[1]				Year 2				Year 3			
	Q1	Q2	Q3	Q4	Q1	Q2	Q3	Q4	Q1	Q2	Q3	Q4
Complete design & build preliminary system	✓											
Order commercial REBCO conductors	✓	✓										
Surface characterization	✓	✓	✓			✓						
Surface preparation			✓									
Joining studies of REBCO tapes		✓	✓	✓	✓	✓	✓	✓	✓	✓	✓	✓
Structure and property characterization						✓	✓	✓	✓	✓	✓	✓
Optimization of EFP variables		✓	✓	✓	✓	✓	✓	✓	✓	✓	✓	✓
EFP system redesign (for HT during EFP)			✓		✓			✓				

II. Accomplishments

Acquisition of REBCO tapes

REBCO tape samples were obtained from a variety of commercial sources, including SuperPower, Inc., American Superconductor Corporation, SuperOx, Sunam, and Theva. Details of each tape, as reported by the manufacturer and as measured by us, are in Table 2.

[1] Note that Year 1 is 11 months, from 5/1/14 – 3/31/15, and Year 2 is from 4/1/15-3/31/16.

Table 2: REBCO Tapes Obtained								
Company	**Amount Received**	**Width (mm)**	**I_c (A, 77 K)**	**Composition**	**Substrate + REBCO thickness (µm)**	**Ag layer (µm)**	**I_c (A, 77 K) Measured**	**RMS Roughness (nm) Measured**
SuperPower	5 m x2	12	387	Y(Gd)BCO/ Al_2O_3-LMO-MgO-LMO-CeO_2/Hastelloy	52	2	382	91.5
SuperOx	1m x1	12	400	REBCO/ Al_2O_3-LMO-MgO-LMO-CeO_2/ Hastelloy C276	65	2	392	61.5
SuNAM	5m x1	12	768	GdBCO/Al_2O_3-Y_2O_3-MgO-LMO/SUS	105 + 1.4	1.5	827	90.6
AMSC (ASC-64)	(separate pieces)	10	380	Y(Dy)BCO/Y_2O_3 -YSZ-CeO_2/Ni5W	75 + 1.2	1	344	24.3
AMSC (ASC-65)	(separate pieces)	10	380	Y(Dy)BCO/Y_2O_3 -YSZ-CeO_2/Ni5W	75 + 1.2	0	-	29.0

Characterization of REBCO Tapes

Properties of YBCO tapes from SuperPower were measured, including I_c(77 K, self-field) and room temperature resistivity. Results are included in Table 2. SuperPower tapes were used for initial studies primarily because they were the first tapes received and because their "quick-ship" option implied that we could regularly and reliably obtain short lengths in the future.

We studied the effects of deoxygenating and reoxygenating tapes as a precursor to studying the effects of oxygen content on EFP bonding. Results (Table 3) show that we are able to readily remove oxygen and subsequently reintroduce oxygen without reducing tape J_c. X-ray diffraction was also used to confirm the transition to the under-oxygenated tetragonal phase and back to the fully-oxygenated orthorhombic phase.

Table 3: Pre- and Post-Processing J_c (kA/mm^2)		
	As Received	Processed
J_c	31.8	30.1
n-value	40	39

The microstructure, roughness, and composition of the surfaces of each manufacturer's tapes were characterized using scanning electron microscopy (SEM) and atomic force microscopy (AFM), and x-ray photoelectron spectroscopy (XPS) was used to examine surface composition of SuperPower tapes. As shown in Figure 1, SuperPower, SuNAM, and SuperOx tapes were coated in a layer of large surface particles, while AMSC tapes displayed a homogeneous surface. EDS implied that most of these surface particles were Cu rich, although the rectangular particles appear to be a-axis oriented REBCO. The XPS spectrum of the SuperPower conductor indicated that these surface structures may be metal oxides; in particular, Y_2O_3 and BaO. Due to the oxide nature of YBCO, however, distinguishing the difference between metal-oxygen bonds in metal oxides and YBCO is difficult and additional analysis techniques would be needed to definitively identify phases. The RMS roughness values as measured by AFM are reported in Table 2.

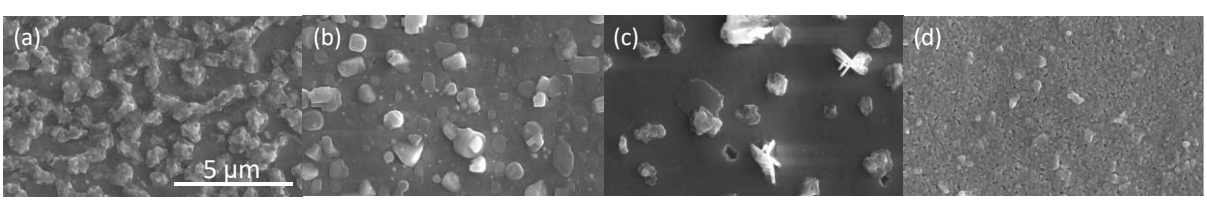

Figure 1: Surface images of the REBCO layer in (a) SuNAM, (b) SuperOx, (c) SuperPower, and (d) AMSC tapes.

Because the initial studies of the tape surfaces showed them to be very rough, we studied ways to modify the surfaces to improve contact during EFP. The initial study used dry polishing with aluminum oxide lapping paper and a methanol rinse. SEM and AFM were performed along with energy-dispersive X-ray spectroscopy (EDS) to confirm that surface particles were removed and roughness decreased without removing the YBCO layer. SEM images in Figure 2 illustrate the improvement; AFM indicated a decrease in average roughness to 21 nm and 9 nm for 0.3 µm and 5 µm lapping paper respectively. Transport measurements showed that polished tapes retained an I_c of 411 A, well above the standard product I_c, indicating that the HTS layer remained undamaged.

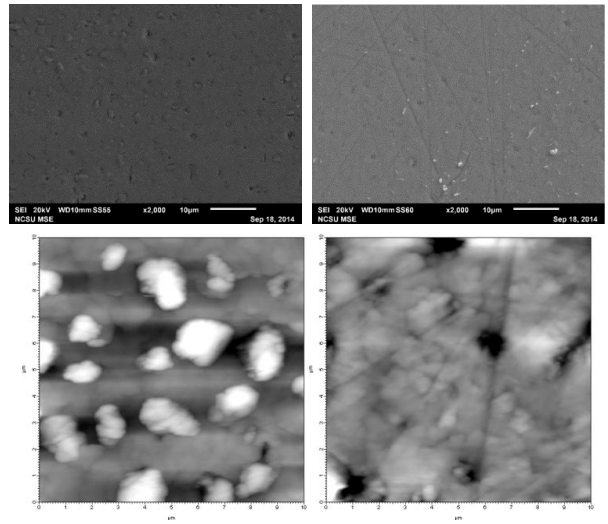

Figure 2: SEM and AFM images of SuperPower tapes polished with 0.3 and 5 µm lapping paper.

Stage 1: Preliminary Tests of EFP Parameters at Room Temperature

Electric field processing experiments were performed that varied the following processing parameters: current density, applied pressure, time for which current was applied, and surface preparation. These conditions were varied for both fully oxygenated and partially de-oxygenated tapes. An experimental matrix is shown in Table 4 indicating the various combinations of parameter values tested.

Each experiment was evaluated first by whether or not it produced a mechanically sound bond, a criteria which requires that the top tape in the lap joint can be picked up and the bottom remains attached. Based on this standard, we found that a higher current density was required to join fully-oxygenated tapes as opposed to those whose oxygen content had been decreased via annealing, and that the joints between oxygenated tapes tended to be mechanically weaker. Subsequent tests in this investigation focused primarily on joining deoxygenated tapes. Furthermore, it became apparent that current density was critical to joint formation. This conclusion was supported by two

Table 4: Preliminary Variation of EFP Parameter Variation (Tapes from SuperPower, Inc., EFP done at room temperature)

Run	Pressure (MPa)	$J_{applied}$ (A/mm^2)	t (s)	Oxygenation	Surface Prep	Breakdown Voltage (V)	Bonded	
1	12	0.238	30	Deoxygenated	none	-	✓	Current Density Variation
2	12	0.475	30	Deoxygenated	none	-	✓	
3	12	0.475	30	Oxygenated	none	-	×	
4	12	0.857	30	Deoxygenated	none	19.5	✓	
5	12	0.857	30	Oxygenated	none		✓	
6	140	0.057	30	Deoxygenated	none	-	×	Pressure tests
7	140	0.379	30	Deoxygenated	none	-	✓	
8	140	0.379	30	Oxygenated	none	-	×	
9	12	0.857	300	Deoxygenated	none	18.3	✓	Time variation
10	12	0.857	300	Oxygenated	none	-	✓	
11	12	0.857	300	Deoxygenated	0.05 µm polish	17.5	✓	Incorporate surface prep (polishing)
12	12	0.857	300	Oxygenated	0.05 µm polish	12.2	×	
13	12	0.857	300	Deoxygenated	0.3 µm polish	16.2	✓	
14	12	0.857	300	Deoxygenated	5 µm polish	20.6	✓	

experiments. First, when adapting our experimental setup to accommodate higher pressure, the available current density available to was limited to 0.379 A/mm^2; tests that maintained this order of magnitude produced a joint, but run 6, in which current density dropped to 0.057 A/mm^2, did not. Second, an additional test was run in which the original 12 MPa system was used to apply a 3x10^5 V/cm electric field to the tapes without current. Although this field is more than twice that which was required for runs that used current, it did not result in any bonding. Qualitatively, we also found that applying the current for a longer duration produced joints that were mechanically stronger, i.e. better able to withstand additional handling.

The behavior of the tapes during processing also indicated that surface effects may be a significant factor. Electrical behavior during EFP for the 12 MPa experiments was measured; in a representative case, the current and voltage increased until electrical breakdown, at which time the voltage dropped to ~1.4 V and the current jumped as high as the power supply allowed, 1.80 A.

The most notable difference between the low and high pressure experiments was the voltage at which breakdown occurred; this is detailed in Table 4, but generally when the pressure was 12 MPa, the breakdown voltages ranged from 12-25 V, whereas when the pressure was increased to 140 MPa, the breakdown voltages ranged from 8-12 V. Note that those values are for essentially identical tapes, so the change in pressure indicates a change in the interface between the tapes and the effective capacitance. This result led to the preliminary surface preparation study presented above, based on the clear dependence of breakdown voltage on pressure as well as the broad range of breakdown values, both of which indicate that the surface plays a large role.

Using a low-temperature four point probe system, electrical measurements of these joints were taken at 77 Kof these joints which indicated that the bonds were ohmic in nature. An SEM image and EDS map of the cross-section of one of the joints, as seen in Figure 3, revealed that the large current used in these tests actually melted the substrates of the two tapes, creating a purely metallic and resistive bond.

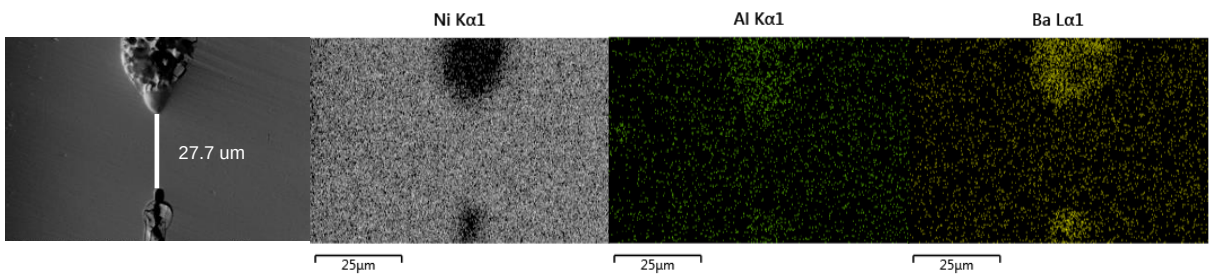

Figure 3: Cross-sectional SEM image and EDS map of a joint processed at room temperature.

Interpretation of Stage 1 Results

Initial results clearly indicated that the surface roughness of SuperPower tapes were a limiting condition for direct EFP joining at room temperature. Furthermore, the metallic bonds created appeared to be a result of extensive Joule heating; therefore, it seemed important to elevate the conductor temperature during EFP to decrease the resistance of the samples.

Stage 2: Pressure and Voltage Variation at Elevated Temperatures

In order to facilitate higher temperatures during bonding, two more iterations of a bonding device were designed and machined. The second, machined out of Hastelloy and insulating ceramic sleeves, is shown in Figure 4; the first had a similar design but contained copper and stainless steel and therefore oxidized heavily above ~500 ºC. The weight of the top plates controlled the pressure (with a maximum of 6.8 MPa) applied to the 3 mm diameter circular electrodes, and detachable current leads

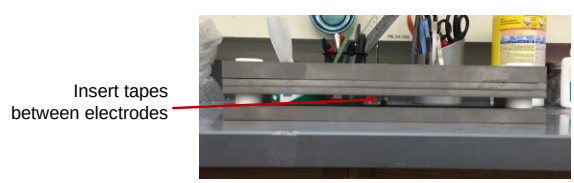

Figure 4: Image of the high temperature EFP rig. Top plates applied controlled amounts of pressure while detachable current leads allowed for voltage/current application. The system operated within a tube furnace.

facilitated voltage and current application. The entire system fit inside a tube furnace. Initially, bonds were attempted at temperatures ranging from 300-650 ºC. However, following the same procedure as the room temperature runs produced no joints, so the range was increased to 700-835 ºC. In addition to temperature elevation, we began limiting the applied voltage to 3 V to prevent breakdown of oxide layers and excessive Joule heating and substrate melting. At these high temperatures, we began placing pressed graphite pellets between the electrodes and the back of the tapes to prevent bonding between the Hastelloy of the bonding rig and the Hastelloy substrate of the SuperPower tapes.

When the voltage was limited and the temperature increased to the 700-835 ºC range, joints were produced over areas approximately 200 x 300 um; a surface image of one of these bonded areas is shown in Figure 5a. A raised layer of REBCO pulled from one tape to the other is clearly evident in these images. When pulling the tapes apart, the joints tended to fail within the buffer stack, as indicated by EDS which showed residual Al on one of the tapes and residual Mg on the other. Due to the delicate nature of the ceramic films, cross-sections of these raised, bonded regions were prepared by focused ion beam (FIB). Preliminary imaging and EDS of these cross-sections, shown in Figure 5b, was promising, demonstrating direct REBCO contact and relatively even elemental distribution.

a)

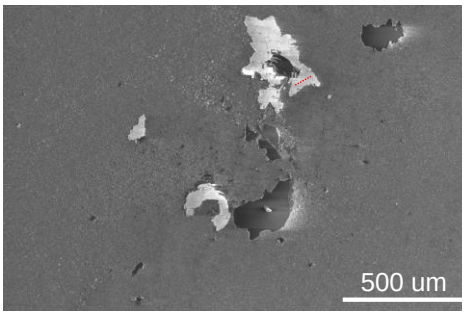

b)

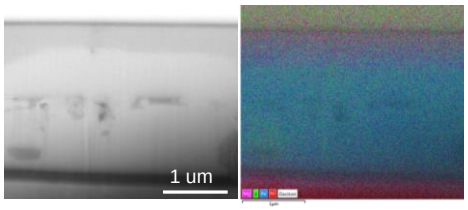

Figure 5: a) Top-down image of a joined region after tapes have been pulled apart. Red line demonstrates type of cross-sectional sampling during FIB. b) Cross-sectional SEM and EDS of a joint prepared by FIB.

At this point, attempts were made to increase the area over which the joints formed with the intention of improving the mechanical strength of the joints. A bonding temperature of 750 ºC had been determined to reliably produce joints, and was therefore used for these pressure/area variation tests. The change in contacted area was facilitated by placing a 1 x 1 cm intermediary Hastelloy block between the tapes and the 3 mm electrodes. Increasing the area while using the same pressure application system reduced the pressure by a factor of ten, which makes direct comparison difficult; however, within these tests the change in pressure distribution decreased the size of the central joint region roughly by a factor of two. Additional small bonded regions, ~5 x 5 um in size, appeared across some parts of the contacted tape. Top-down images of these two types of bonds are depicted in Figure 6.

Electrical testing was attempted on these joints; however, their mechanical instability made the task nearly impossible. The few measurements obtained at 77 K indicated that the joints behaved dielectrically until breakdown, at which point they behaved ohmically.

a)

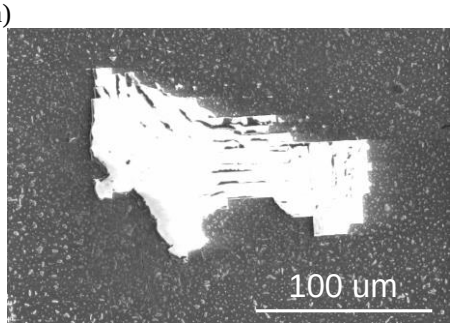

b)

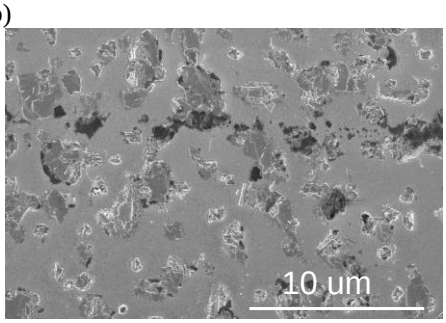

Figure 6: The decrease in applied pressure and increase in contacted area a) decreased the size of the central bonded area and b) created smaller bonded regions found on selected portions of tape.

Interpretation of Stage 2 Results

The issues producing metallic joints were side-stepped by applying sufficient temperatures with a low enough applied field. A balance was struck between the thermal and electric driving forces in play and the ability of the atoms in the film to respond, resulting in this project's first REBCO/REBCO bonds. Additionally, the joints' responses to the changes in pressure application highlighted two important concepts moving forward. First, a larger contacted area would be required to produce bonding over a greater area. Second, the magnitude of pressure would need to be maintained for each discrete bonded area to attain a practical size. Furthermore, the electrical measurements indicated two more

concerns: that the poor mechanical behavior of the joints was going to inhibit the necessary electrical testing, and that oxygen content may be an issue despite relatively low processing conditions, as indicated by the poor conductivity at 77 K.

Stage 3: Pressure-assisted Bonding at Elevated Temperatures

At this stage, the applied pressure presented itself as a significant roadblock, both because it theoretically limited the potential current transfer capability of the joint and because it reduced the mechanical robustness of the joint by concentrating any external forces on a small area. To facilitate greater pressures over a larger area, the rig shown in Figure 7 was designed and built. The electrodes this time were a 1 x 1 cm square, although this area was reduced slightly by the use of the circular 1 cm diameter graphite pellets, mentioned earlier, to prevent sticking between the electrodes and the tape. The torque applied to the bolts holding the two plates together was controlled for each test and measured using a precision torque wrench, allowing for the calculation of the applied pressure. It is important to note that this number functioned only as a starting estimate, due to the thermal expansion of the metal during the EFP process.

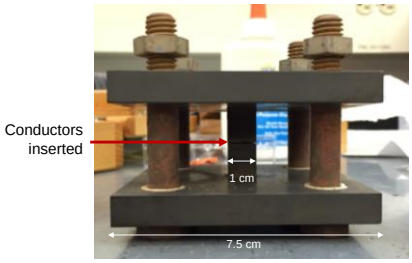

Figure 7: Image of the second high temperature EFP rig. Ti bolts applied controlled amounts of pressure while detachable current leads allowed for voltage/current application. The system operated within a tube furnace.

Comparison of joining different manufacturers' tapes

Using this new system, joints were attempted between tapes from all four manufacturers using pressures of 60 and 150 MPa and temperatures of 600 and 750 ^{o}C. If an electric field was applied, the safe 3 V value was used, typically resulting in currents of 4-6 A. The anneal (and voltage, if applicable) time was one hour and an O_2 atmosphere was used in an attempt to prevent decreased O stoichiometry. Due to the relatively rough surfaces of the commercially produced tapes, smooth (6 – 10 nm roughness) REBCO films grown by Theva on sapphire substrates were purchased. The pressures applied to the smooth films were limited due to the brittle substrate. In order to electrically test the resulting joints, an insulating epoxy encased the joints to stabilize them mechanically. The electrical measurements were performed either in a physical property measurement system (PPMS) or using a four-point probe system with a high current supply in a cryostat.

When these parameters were applied, we found that all of the conductors bonded at 750 ^{o}C, while only AMSC and SuNAM tapes bonded at 600 ^{o}C; in this study, there were no obvious effects based on the inclusion or exclusion of the electric field. Cross-sections of each conductor, as prepared by FIB and imaged in an SEM, were compared between manufacturers for microstructure and chemical homogeneity and correlated to the joints' electrical behavior down to 4 K.

The microstructures for each manufacturer are shown in Figure 8 and the corresponding resistance measurements are shown in Figure 9. SEM and EDS of SuNAM cross-sections showed a significant interlayer of a Cu-rich phase between the REBCO layers. SuperPower and SuperOx showed mixed interfaces with some homogeneous REBCO areas and other areas with elemental segregation. Only AMSC joints showed consistently homogenous interfaces. All conductors exhibited a drop in resistance around 90 K. SuNAM retained a high resistance value below this temperature, while AMSC exhibited a second drop to nearly zero resistance around ~68 K. Both SuperPower and SuperOx showed a second transition around this temperature as well as a third transition to near zero resistance between 16 and 60 K. Attempts to measure transport I_c at 4.2 K of each joint, however, indicated poor or non-existent superconducting transitions in all samples but AMSC, implying poor connectivity through the joint.

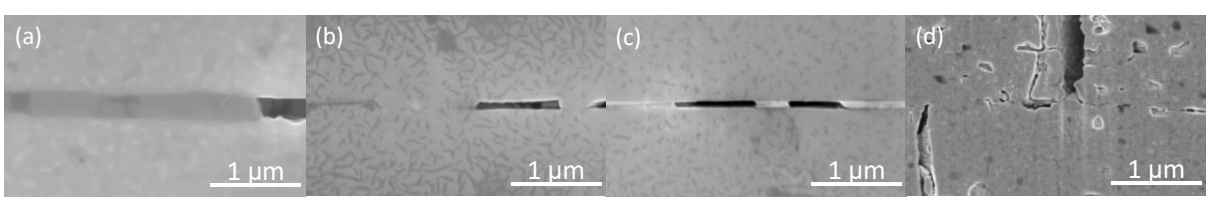

Figure 8: Cross-sections of bonded conductors for SuNAM (a), SuperOx (b), SuperPower (c), and AMSC (d) conductors.

Bonding further explored through AMSC results

Based on these results, the bonding process was explored further with a focus on AMSC conductors. The first thing observed from bonding experiments with AMSC conductors in various conditions was a clear temperature/pressure regime. At 600 ºC, AMSC conductors required a higher pressure to bond than conductors processed at 750 ºC. Interestingly, none of the other conductors exhibited this behavior. Neither SuperOx nor SuperPower bonded at 600 ºC even under the highest pressure studied here. The Theva films also did not bond at 600 ºC, although high pressure was not applied in that case. Once bonded, however, the microstructures at the interface and across the surface appeared unaffected by the choice of processing temperature or the application of electric field.

Close investigation of an AMSC joint revealed a homogeneous bond lacking any phase or elemental segregation at the joint interface. Some interfacial pores were present, indicating incomplete bonding between the surfaces; note that the pores throughout the bulk are characteristic of AMSC conductors before any additional processing. These bonds tended to form over an area of approximately 0.01-0.08 cm^2, 1.3-10.2% of the nominally contacted area. The spread in joint size likely resulted from variations in pressure application during bonding; although the same rig was used to obtain these results, neither the plates nor the conductor surfaces were perfectly flat, and some variation in the way they met almost certainly occurred. Notably, the un-joined portions were also affected by the process. Specifically, a severe crack pattern was evident in top-down SEM images of the conductors post-bonding. The cracks extended across much of the contacted surface and permeated to the substrate in most cases.

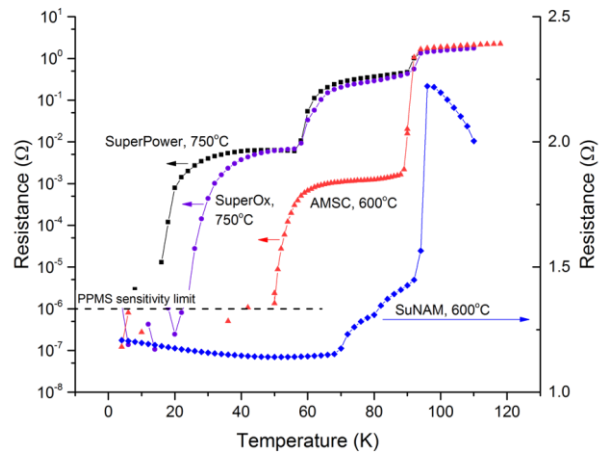

Figure 9: Resistance versus temperature for joints between conductors from each manufacturer. The dotted line indicates the sensitivity limit of the PPMS used for the measurements.

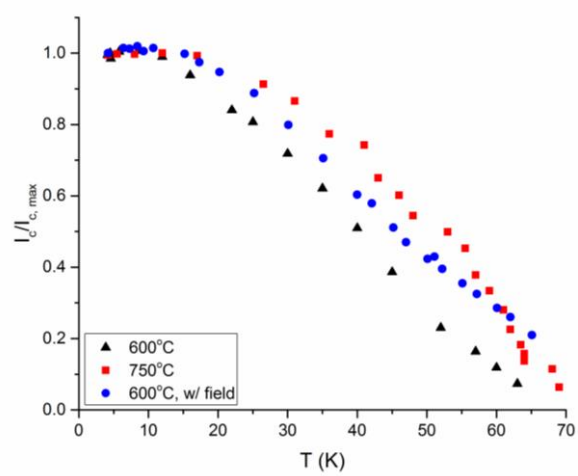

Figure 10: I_c normalized by I_{cmax} vs. temperature for AMSC joints processed at 600 ºC with and without electric field, and at 750 ºC without electric field.

Four-point probe measurements on several AMSC joints yielded I_c values varying from 0.5 to 20 A at 4.2 K. A series of I_c measurements performed as temperature increased and normalized by $I_{c,\,max}$ implied a depressed T_c of ~68 K, as shown in Figure 10. This represented a more accurate measurement than that of the PPMS due to temperature sensor placement and cooling methods. Conductors processed at both 600 and 750 ºC, with and without electric field, demonstrated similar I_c and T_c values.

Additional measurements extracted the characteristics of the film bulk from the joined interface. First, the magnetic response was measured in a SQUID MPMS over a range of temperatures for both SuperPower and SuperOx conductors after joining. The bulk of the films retained a T_c around 90 K. Similar magnetization measurements on AMSC conductors were not useful due to the magnetism of the Ni-5W substrate; instead, an alternate approach measured the in-plane resistance in the PPMS of a single AMSC conductor subjected to the 750 ºC heat treatment with its HTS layer exposed. The resistance retained a 90 K superconducting transition in the PPMS, and the previously observed second drop was notably absent.

The chemical distinctions between the bulk and joint interface were elucidated by ToF-SIMS results shown in Figure 11. The depth profiles revealed a small concentration of Ni on the conductor surface after etching; the

annealed sample showed that Ni from the surface diffused into the first few hundred nanometers of the REBCO layer during heating. A slight O gradient was also present, with the lower concentration at the surface. An XPS spectrum, however, found no presence of Ni, indicating that the surface Ni concentration of one of the etched tapes was below 0.1%.

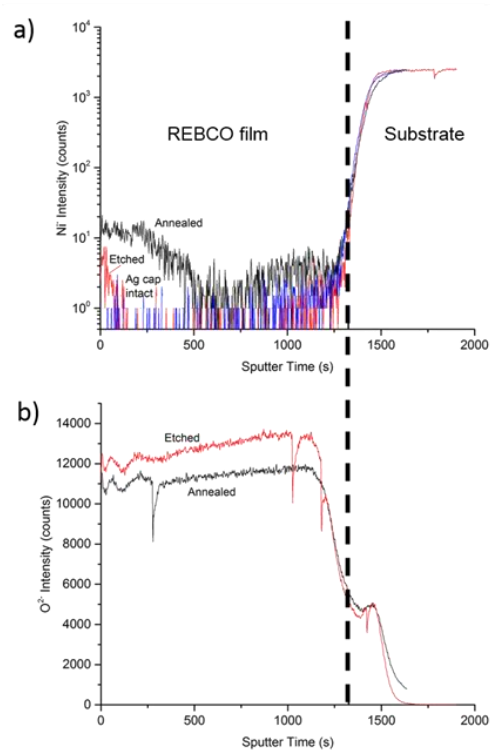

Figure 11: TOF-SIMS depth profiles of (a) Ni and (b) O ions for AMSC REBCO layers with the Ag cap intact, after etching, and after etching and quench annealing to 600 ºC.

Interpretation of Stage 3 Results

Comparison of joining different manufacturers' tapes

Correlating interfacial purity with electrical behavior across manufacturers, it was apparent that the most important surface characteristic for REBCO bonds was the purity of the starting surface, including both large particles such as the Cu phase on the SuNAM conductors as well as unintentional "dopants" such as the Ni found on the AMSC REBCO surfaces. For instance, the temperature dependence of the resistance of the SuNAM joint followed the behavior expected of an HTS/Cu oxide composite; that is, resistance increased with temperature until the T_c of REBCO, at which point the semiconducting behavior of the Cu oxide dominated the measurement. On the opposite end of the spectrum, the sharp dual transitions of the AMSC joint correlated well to a superconducting bulk/interface structure with a retained bulk and depressed interfacial T_c.

An intriguing disconnect existed between the way the morphology of AMSC conductors and conductors from other manufacturers facilitated the bonding process. As mentioned previously, AMSC and SuNAM conductors bonded at significantly lower temperatures than SuperPower and SuperOx conductors. The bonding of SuNAM conductors was not directly comparable to the others due to the isolation of the REBCO surfaces by the Cu oxide surface coat, and will therefore be excluded from this portion of the discussion. Qualitatively correlating the homogeneity of the bonded interface for the different conductors with the surface roughness values in Table 2, it is tempting to claim that film smoothness may be responsible for this disparity. Yet, if only a critical RMS roughness was required, the smooth films on wafers would also have bonded at 600 ºC. Rather, the distinction appeared to originate from the effectiveness of pressure-assisted sintering applied to AMSC as opposed to SuperPower and SuperOx.

Pressure-assisted sintering occurs when microscopic features such as pores locally amplify the macroscopic stress applied to the system. Pressure assistance was required to bond AMSC conductors at 600 ºC, but the effect did not extend to SuperPower and SuperOx conductors. This identified microstructural differences, not smoothness, as responsible for the difference in bonding temperature. AMSC's morphology was characterized by small round features arranged in gradual slopes, not unlike a desert landscape. In contrast, SuperPower and SuperOx surfaces were characterized by relatively flat films with large particles irregularly spaced across the surface. In the case of interfaces, pores are created by frequent but disconnected points of contact between the two surfaces, similar to the way particles contact each other in a green pressed pellet. If each surface feature provides one possible point of contact (at its highest point from the film surface), then it becomes clear that small, densely packed features provide significantly more interfacial points of contact and therefore pores than large features that are less densely located. A fine-featured surface then, such as AMSC's, not only enables pressure assistance in sintering, but also provides improved degrees of contact between surfaces. In fact, in the case of smooth surfaces with effectively no features, contact can be easily foiled by imperfections in the processing atmosphere such as dust.

Bonding further explored through AMSC results

Assessing the merits of this approach to superconducting joints required more context than a simple statement of critical parameters. At face value, the parameters reported above were significantly depressed as compared to the

parent conductor, but there were several reasons for this, some of which are related to the bonding process and some which are not. To begin, there are a couple of possible contributions for the several orders-of-magnitude reduction in I_c. First, the lap joint nature of the bond requires that the current at least briefly travel along the c-direction in the REBCO crystal structure. The anisotropy of REBCO's properties are well established; in fact, the anisotropy factor was recently measured to be 500-600, decreasing the critical current density (J_c) of 2G conductors from 2.2 MA/cm^2 to 4 kA/cm^2 at 77 K[1]. Without J_c values for the joints discussed here, it is difficult to assess the quality of the interface with respect to current carrying capacity. Although area values can be estimated from joints imaged after testing, visual measurement does not account for portions of the joint which either break during cooling or are isolated due to cracks. From an engineering perspective, a more useful figure of merit could be defined as the ratio of joint I_c to the a-b plane parent I_c, indicating fractional I_c retained; however, this parameter does not account for the effect of mechanical degradation of the film in the joint region. These cracks may reduce the current-carrying capacity of the parent film, restricting the current which actually reaches the bonded region.

The other critical parameter reduced during the joining process was T_c. Commonly, T_c reduction indicates a reduced oxygen stoichiometry; yet the low temperatures and O_2 atmosphere this process utilizes should prevent oxygen loss. YBCO thin film stability studies state that the conductors should not have undergone the orthorhombic/tetragonal transition which accompanies O_2 loss under these conditions, and the process remains well below either the decomposition or peritectic temperatures of the system[2]. Furthermore, the bulk retention of T_c as measured by SQUID and resistance measurements implied the source of T_c depression was relegated to a thin interfacial layer. The transverse PPMS measurements of the AMSC joints in Figure 3 supported this idea; the first resistance drop corresponded to the bulk T_c of 90 K, whereas the second demonstrated that the conductor had been damaged somewhere else along the current path. Neither SQUID nor PPMS allowed for further probing of the possibility of conductor with spatially relegated chemical changes. The origin of the depressed transition was ultimately diagnosed by the ToF-SIMS ionic depth profiles. The ion distributions depicted in Figure 7 highlight two potential causes of low T_c: Ni in the first few nanometers of the film, and an oxygen content which decreases across the film. Ni is commonly said to "poison" REBCO; specifically, it dissolves into the structure and occupies some of the Cu sites, which is correlated with depressions of T_c down to 60 K depending on concentration[3]. While this effect should not be ignored, the observed T_c of 68 K would require that Ni occupy 8.2% of the Cu sites or 2% of a YBCO film; the XPS results confirmed that the surface concentration was below 0.1%[3]. Given the insufficiency of the Ni concentration as the main source of T_c depression, the decreasing O content uncovered in SIMS was revealed as the main culprit. Assuming the REBCO near the substrate remained at full oxygen stoichiometry (x = 0) and the low content at the surface limited the T_c (corresponding to x = 0.29), a linear variation would have allowed ~620 nm of REBCO to retained full T_c[4]. This agrees well with the in-plane resistivity measurements, which indicate the availability of an in-plane current path with 90 K T_c.

Overall, this stage elucidated a couple of key elements and remaining questions surrounding the bonding process. First, chemically clean surfaces were crucial to achieving joints capable of conducting supercurrent. Second, although high uniaxial pressures reduced the temperatures required to bond films, the benefit was nullified by the accompanying mechanical degradation. In addition, although the films did suffer oxygen loss and resulting T_c depression, the degree of loss appeared unaffected by the choice of 600 or 750 ºC. The resulting T_c still remained above the operating temperature of many superconducting magnets even without a post-joining anneal. Finally, the inclusion of an electric field provided no observable benefit; it was postulated that the high pressures and resulting creep-based mechanisms overpowered any effects.

Table 5. Results of Low Pressure Tests

Temperature (C)	Time (min)	Field application	Bonds?
750	24*60	-	✓/✓
	24*60	3V during anneal	✓/✓
700	24*60	-	✓/✓
	24*60	3V during anneal	✓/✓
750	6.5*60	-	✓
	6.5*60	3V during anneal	✓
750	60	-	✓/✓
	60	3V during anneal	✓/✓
700	60	-	✓/✓
	60	3V during anneal	✓/✓
650	60	-	✗/~✓
	60	3V during anneal	✗/~✓
700	12	-	✗/✓
	12	3V during anneal	✓/✓
700	6	-	✓
	6	3V during anneal	✗

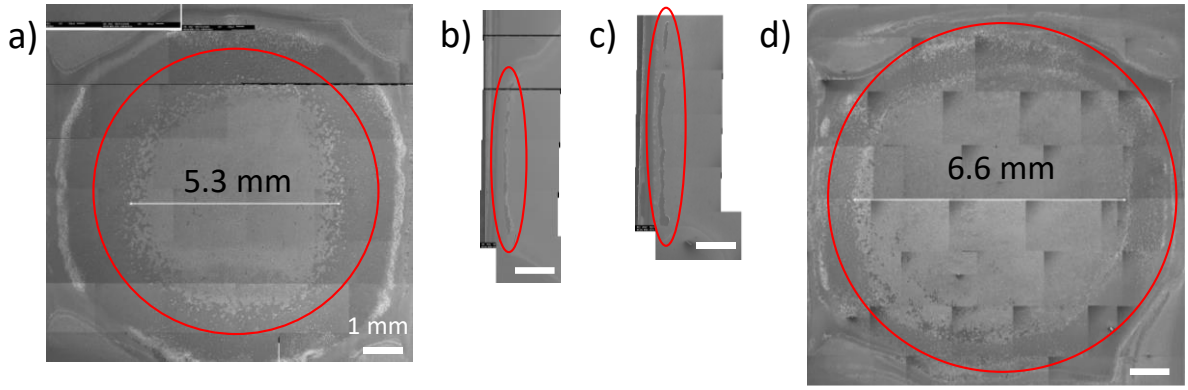

Figure 12: Top-down image of joined regions processed at a) 750 ºC for 24 hours, b) 700 ºC for 24 hours, and c) 750 ºC for 1 hour without an electric field and d) at 750 ºC for 24 hours with electric field. Joined regions are circled in red for visual clarity. Sample (b) also possessed several small bonded regions in the tape's center which are not visible at this magnification.

Stage 4: Low Pressure Bonding at Elevated Temperatures: A Look at Kinetics

Moving forward, we aimed to answer two main questions: 1) what was limiting the size of the joined area and 2) were there any benefits from electric field application waiting to be reaped? Both of these questions centered around exploring whether the limitations on the process as developed were kinetic in nature. As such, temperatures and times were varied and investigated for changes in joint size and microstructure. In addition, a second rig was machined, structured like the one shown in Figure 7, which allowed for simultaneous processing of one joint with an electric field and one processed only with heat. This set of tests used exclusively AMSC tapes due to their preferred surface characteristics and were performed with only 6 MPa of starting pressure. Temperatures of 650, 700, and 750 ºC were applied for anneal times of 6 minutes, 12 minutes, 1 hour, and 24 hours.

Table 5 summarizes the parameters applied and the success or failure of a mechanically observable joint. Multiple check marks or x's indicate the number of samples run at those conditions. Lower temperatures and shorter times tended to not reliably produce joints. Longer times did improve the reliability of joint production, but the sizes of the joints produced for long times at different temperatures stood in stark contrast to each other, as shown in Figure 12 (a-c). Low temperature samples held for long periods of time were comparable to higher temperature samples held for short periods of time. These samples held for a longer time also appeared to fracture differently than previously produced joints. While joints during previous stages tended to fracture somewhere within or at the interface of the buffer stack, the joints from this study fractured at the buffer stack in some areas and within the REBCO films themselves at others.

Within the same set of processing conditions, there did appear to differences between samples processed with and without the electric field. The most obvious dissimilarity was the joint size, as evidenced by a comparison between Figure 12 (a) and (d). Additionally, higher magnification images of the lower temperature samples showed that small bonded areas had formed on the electric field samples in greater size and number than on the purely heat treated samples. Finally, the joints processed with and without an electric field seemed to fracture slightly differently. While both fractured within the REBCO film at points, the areas where they fractured at the Hastelloy/buffer stack interface displayed different microstructures, as shown in Figure 13. It appeared that the substrate possesed a layered structure

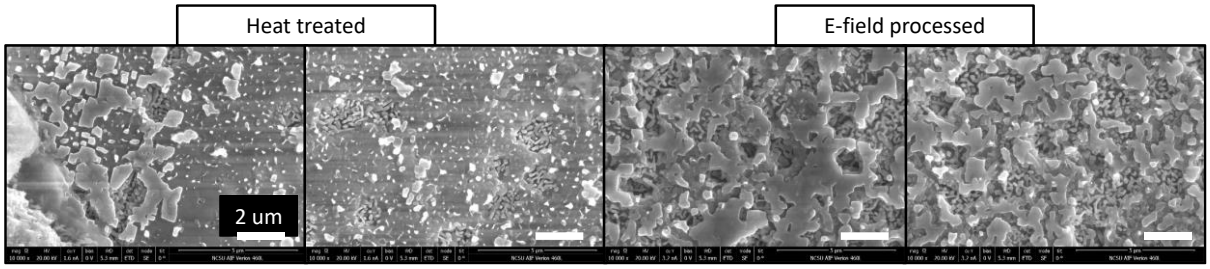

Figure 13: Hastelloy fracture surfaces of samples processed at 750 ºC for 24 with and without electric field.

where a dense overlayer covered a more porous portion of the substrate; the electric field samples then removed more of the overlayer during fracture.

Interpretation of Stage 4 Results

Our observations of time and temperature effects on joint size in these samples are qualitatively consistent with an Arrhenius type of growth, in which the growth rate is proportional to $\exp\left(-\frac{Q}{kT}\right)$ and Q represents the activation energy for diffusion while kT represents thermal energy. Additional time always allowed the joint size to grow larger, but increasing the temperature by small amounts had a more significant (qualitatively exponential) effect. Within this framework, we then suggest that the observed electric field effects can be attributed to a decrease in the activation energy term Q; this explanation would accommodate the larger joint size on electric field samples processed for 24 hours and the increased number of small joined regions on the lower temperature electric field samples. There is also limited evidence to suggest that the bonding within the Hastelloy/buffer oxide/REBCO stack is affected and possibly improved by the electric field. These concepts should be more fully explored however, before definite conclusions are reached.

III. Additional Information

Publications: "Solid State Bonding of (RE)$Ba_2Cu_3O_{7-x}$ Coated Conductors and the Impact of Surface Morphology in Producing Superconducting Joints," submitted to *Superconductor Science and Technology* on April 18th, 2017 (attached).

Posters were presented at the 2014 Applied Superconductivity Conference, the 2015 Electronic Materials and Applications Conference, the 2015 Magnet Technology Conference, and the 2015 European Conference on Applied Superconductivity, in addition to oral presentations at the 2016 Applied Superconductivity Conference and the 2016 and 2017 Electronic Materials and Applications Conferences. All presentations acknowledged Department of Energy support under this contract.

Personnel: In addition to the PI, this contract supported a graduate student in the Department of Materials Science and Engineering, Mrs. Carolyn Grimley. Her appointment is a standard ½-time graduate research assistantship. A full-time post-doctoral researcher, Dr. Menghui Liu, was also funded for one year. Another graduate student, Mr. Weston Straka, has also been involved, but without support from this contract.

References

[1] Y. Jia, J. Hua, G. W. Crabtree, W. K. Kwok, U. Welp, A. P. Malozemoff, M. Rupich, and S. Fleshler, Superconductor Science and Technology **23** (11), 115017 (2010).

[2] J. S. Kim and D. R. Gaskell, Journal of the American Ceramic Society **77** (3), 753 (1994); R. Cloots, T. Koutzarova, J. P. Mathieu, and M. Ausloos, Superconductor Science and Technology **18** (3), R9 (2005).

[3] Youwen Xu, R. L. Sabatini, A. R. Moodenbaugh, Yimei Zhu, S. G. Shyu, M. Suenaga, K. W. Dennis, and R. W. McCallum, Physica C: Superconductivity **169** (3), 205 (1990).

[4] Jinhua Ye and Keikichi Nakamura, Physical Review B **48** (10), 7554 (1993).

Appendix 1: Manuscript submitted for publication attached

Solid State Bonding of (RE)$Ba_2Cu_3O_{7-x}$ Coated Conductors and the Impact of Surface Morphology in Producing Superconducting Joints

Carolyn Grimley, Chuanzhen Zhou, and Justin Schwartz
Department of Materials Science and Engineering, North Carolina State University, Raleigh, NC 27695-7907
Analytical Instrumentation Facility, North Carolina State University, Raleigh, NC 27695-7531

ABSTRACT

As the manufacturing of high temperature superconductors (HTS) such as (Rare Earth)$Ba_2Cu_3O_{7-x}$ (REBCO) has improved, interest in applications has grown, yet some practical issues still prevent their widespread utilization. One remaining issue is the inability to create superconducting joints appropriate for persistent superconducting magnets. A joining technique would allow for longer lengths of conductor and grading of different HTS materials along the length of the conductor. Previous attempts at persistent current joints focused on the use of full or partial melting of directly contacted REBCO layers. Although successful, the conductor suffered significant oxygen loss and required a lengthy oxygen anneal to restore the superconducting properties. Here, REBCO conductors from four manufacturers are joined using solid-state bonding and characterized for microstructure and electrical behavior. In some cases, the bonding is aided by large uniaxial pressures and/or an electric field. For more porous samples with small surface features, pressure-assisted bonding is accomplished at 600 ^{o}C; denser films with larger, rougher features require higher temperatures to bond. Bonds between films with homogeneous interfaces retain superconductivity with a depressed critical temperature of ~68 K and critical current values ranging from 0.5 to 20 A. The T_c depression is linked to a linear O decrease throughout the film bulk as a result of the heat treatment; full T_c is retained in an estimated 600 nm of the film. The source of the reduced critical current remains uncertain, but factors such as c-axis transport within the joint and crack formation during bonding are discussed. The contribution of surface morphology to bonding is also discussed via comparison between the different surfaces represented by the four manufacturers' conductors.

I. INTRODUCTION

Interest in superconducting joints between high temperature superconductors (HTS) has grown in the last decade as the commercial production of HTS conductors improved and became viable for practical use in high field superconducting magnets. The HTS (Rare Earth)$Ba_2Cu_3O_{7-x}$ (REBCO) in the form of a coated conductor (CC) in particular receives much attention due to its high critical current and mechanical strength.

Two approaches have been studied to create joints between REBCO conductors. The first uses some variation on soldering with a metallic interlayer between the HTS layers of the conductor, the goal being a joint of low resistance. The specific application of the technique includes diffusion bonding of the conductor's Ag stabilizing layer, Cu welds using ultrasonic techniques, and the use of Sn-based solders[1]. Although appropriate for certain applications, such as demountable current leads, resistive joints cannot support magnets requiring persistent current mode due to the heat generation of their normal layer, rendering them unsuitable for use in applications such as magnetic resonance imaging (MRI) [2].

A fully superconducting joint was realized using the second approach: direct bonding of the HTS layers via partial melt processing[3]. In this case, two GdBCO conductors were directly contacted

and heated to 835 ^{o}C in Ar to produce partial decomposition and subsequent bond formation at the interface. A set of micro-holes was then drilled through the conductors, and a post-joining anneal in O_2 restored the joint to full superconductivity. The annealing procedure proved to be the most complicated and lengthy part of the process but appears to be unavoidable for melt-based processes. Similar annealing techniques commonly appear in superconducting joints between REBCO bulk conductors which utilize partial or total melting[4]. REBCO releases O_2 as part of its peritectic decomposition, so a technique requiring melting will typically also require an oxygen-restoring step[5].

Until now, no literature has been published attempting the solid-state bonding of REBCO CCs. Yet even at low temperatures, a driving force for mass diffusion exists due to the imperfect flatness of the conductors. Local variations in curvature, such as those on the surface of REBCO conductors, produce a sintering stress which drives mass from concave portions of the surface to the convex regions[6]. If we consider two similarly shaped films pressed together, such mass diffusion will produce a bonded interface between the two layers. Such diffusion can be enhanced at lower temperatures by the application of additional driving forces such as uniaxial pressure and/or an electric field. In this study, the assistance from high uniaxial pressure appears to dominate any electric field effects. The avoidance of high temperatures and the maintenance of the correct REBCO phase implies great potential in the achievement of a sintered joint between REBCO CCs.

II. EXPERIMENTAL APPROACH

An approach is developed to directly bond the HTS layers of REBCO CCs in a lap-joint geometry. First, an etchant solution of 1:1:4 NH_4OH:H_2O_2:CH_3OH removes the Ag stabilizing layer from the conductors. The exposed REBCO layers are then overlapped and pressed together using the apparatus shown in Figure 1. The screws holding the plates together control the pressure applied according to $P=T/(cDA)$, where P is the pressure, T is the applied torque, c is the coefficient of friction, D is the bolt diameter, and A is the electrode area. Yet this equation provides only an initial estimate as the actual pressure on the conductors increases during processing due to thermal expansion. The entire system fits into a tube furnace through which oxygen flows, and each plate possesses detachable high temperature current leads facilitating the application of an electric field and current during processing.

For this study the processing parameters are binary, with temperatures of 600 ^{o}C or 750 ^{o}C and initial (room temperature) pressures of 60 MPa or 150 MPa. If an electric field is applied, 3 V is used, resulting in a current of 4-6 A. The procedure is applied to conductors from four REBCO manufacturers: American Superconductor (AMSC), SuNAM, SuperOx, and SuperPower. To test the process on smoother films, an additional experiment uses YBCO thin films (200 nm thick) on sapphire wafers obtained from Theva. These experiments use a significantly lower pressure to prevent cracking the sapphire wafers.

The differences in surface roughness and morphology between the various sample types are characterized using scanning probe microscopy (SPM, Bruker Dimension 3000), scanning electron microscopy (SEM, FEI Verios 460L), and energy dispersive x-ray spectroscopy (EDS). Although results using all samples are discussed, many of the experiments focus on bonds between the AMSC conductors due to the apparently phase pure REBCO surfaces and favorable surface morphology.

The joint microstructures are characterized by SEM. Cross-sections are prepared for imaging using a dual focused ion beam (FIB) and SEM. Electrical measurements use a four-point probe within a Quantum Design physical property measurement system (PPMS) in addition to a lab-developed cryostat and high current four-point probe setup. The joints are encased in an electrically insulating epoxy with a low coefficient of thermal expansion before electrical measurements to improve mechanical stability.

To assess changes to the bulk of the films during processing, control conductors are compared to an individual AMSC conductor whose Ag is etched, another which is etched and annealed in oxygen for 1 hour at 600 ^{o}C then quenched, and pieces of conductors which are part of actual joints. Depth profiling of the chemical species of these samples is studied via time-of-flight secondary ion mass spectrometry (ToF-SIMS). Further surface analysis of these samples was also performed using x-ray photoelectron spectroscopy (XPS). The critical temperatures (T_c) of the bulk SuperPower, SuNAM, and SuperOx samples are measured using a Quantum Design superconducting quantum interference device (SQUID) based magnetic property measurement system (MPMS). Due to the ferromagnetism of AMSC's Ni-5W substrate, resistance measurements in the PPMS are used to measure T_c.

III. RESULTS

Surface characterization

A comparison of the conductor surfaces from the four manufacturers reveals vastly different surface morphologies and roughnesses. Figure 2 shows SEM images of each conductor surface while Table 1 reports the root mean square (RMS) roughness values. Conductors from all manufacturers except AMSC possess a significant number of discrete surface particles on the order of 1-2 μm. EDS identifies a Cu-rich phase on the SuNAM and SuperPower conductors; the SuperPower surface also contains a-axis oriented REBCO grains. The particles on the surface of the SuperOx conductor appear to be compositionally consistent with the underlying REBCO film. Following the trend of surface particle impurity, SuNAM and SuperPower conductors are the roughest with 90.6 and 91.5 nm RMS roughnesses, followed by SuperOx with 61.5 nm and AMSC at 24.3 nm. The surface roughness of the Theva thin films are reported by the company as 6-10 nm.

Characteristics of bonding for each conductor

When the joining procedure outlined earlier is applied to conductors from all manufacturers, significant differences emerge in the resulting joint interfaces and electrical behavior. All conductors, including the smooth wafers, bond at 750 ^{o}C, whereas only AMSC and SuNAM conductors bond at 600 ^{o}C. The joint cross-sections are compared in Figure 2, illustrating the microstructural differences between these joints. SEM and EDS of SuNAM cross-sections show a significant interlayer of a Cu-rich phase between the REBCO layers. SuperPower and SuperOx show mixed interfaces with some homogeneous REBCO areas and other areas with elemental segregation. Only AMSC joints show consistently homogenous interfaces.

The temperature dependence of the joints' resistance as measured by PPMS is shown in Figure 3. All conductors exhibit a drop in resistance around 90 K. SuNAM retains a high resistance value below this temperature, AMSC exhibits a second drop to nearly zero resistance around ~68 K. Both SuperPower and SuperOx show a second transition around this temperature as well as a third transition to near zero resistance between 16 and 60 K. Attempts to measure transport I_c at

4.2 K of each joint, however, indicates poor or non-existent superconducting transitions in all samples but AMSC, implying poor connectivity through the joint. Based on these results, the bonding process is explored further with a focus on AMSC conductors.

Basics of the joining process and joint behavior

The first thing observed from bonding experiments with AMSC conductors in various conditions is a clear temperature/pressure regime. At 600 ^{o}C, AMSC conductors require a higher pressure to bond than conductors processed at 750 ^{o}C. Interestingly, none of the other conductors exhibit this behavior. Neither SuperOx nor SuperPower bond at 600 ^{o}C even under the highest pressure studied here. The Theva films also do not bond at 600 ^{o}C, although high pressure was not applied in this case. Once bonded, however, the microstructures at the interface and across the surface appear unaffected by the choice of processing temperature or the application of electric field.

Close investigation of an AMSC joint in Figure 4 reveals a homogeneous bond lacking any phase or elemental segregation at the joint interface. Some interfacial pores are present, indicating incomplete bonding between the surfaces; note that the pores throughout the bulk are characteristic of AMSC conductors before any additional processing. These bonds tend to form over an area of approximately 0.01-0.08 cm^2, 1.3-10.2% of the nominally contacted area. The spread in joint size likely results from variations in pressure application during bonding; although the same system is used to obtain these results, neither the plates nor the conductor surfaces are perfectly flat, and some variation in the way they meet almost certainly occurs. Notably, the un-joined portions are affected by the process. Specifically, a severe crack pattern is evident in top-down SEM images of the conductors post-bonding. The cracks extend across much of the contacted surface and permeate to the substrate in most cases.

Four-point probe measurements on several AMSC joints yield I_c values varying from 0.5 to 20 A at 4.2 K. A series of I_c measurements performed as temperature increased and normalized by $I_{c,max}$ implied a depressed T_c of ~68 K, as shown in Figure 5. This represents a more accurate measurement than that of the PPMS due to temperature sensor placement and cooling methods. Conductors processed at both 600 and 750 ^{o}C, with and without electric field, demonstrated similar I_c and T_c values.

Additional measurements extract the characteristics of the film bulk from the joined interface. First, the magnetic response is measured in a SQUID MPMS over a range of temperatures for both SuperPower and SuperOx conductors after joining. The bulk of the films retain a T_c around 90 K, shown in Figure 6a. Similar magnetization measurements on AMSC conductors are not useful due to the magnetism of the Ni-5W substrate; instead, an alternate approach measures the in-plane resistance in the PPMS of a single AMSC conductor subjected to the 750 ^{o}C heat treatment with its HTS layer exposed. The resistance, shown in Figure 6b, retains a 90 K superconducting transition in the PPMS, and the previously observed second drop was notably absent.

The chemical distinctions between the bulk and joint interface are elucidated by ToF-SIMS results shown in Figure 7. The depth profiles reveal a small concentration of Ni on the conductor surface after etching; the annealed sample shows that Ni from the surface diffuses into the first few hundred nanometers of the REBCO layer during heating. A slight O gradient is also present,

with the lower concentration at the surface. The XPS spectrum found no presence of Ni, indicating that the surface Ni concentration was below 0.1%.

IV. DISCUSSION

Role of surface characteristics in bonding

Correlating interfacial purity with electrical behavior across manufacturers, it is apparent that the most important surface characteristic for REBCO bonds is the purity of the starting surface, including both large particles such as the Cu phase on the SuNAM conductors as well as unintentional "dopants" such as the Ni found on the AMSC REBCO surfaces. For instance, the temperature dependence of the resistance of the SuNAM joint follows the behavior expected of an HTS/Cu oxide composite; that is, resistance increases with temperature until the T_c of REBCO, at which point the semiconducting behavior of the Cu oxide dominates the measurement. On the opposite end of the spectrum, the sharp dual transitions of the AMSC joint correlate well to a superconducting bulk/interface structure with a retained bulk and depressed interfacial T_c.

An intriguing disconnect exists between the way the morphology of AMSC conductors and conductors from other manufacturers facilitate the bonding process. As mentioned previously, AMSC and SuNAM conductors bond at significantly lower temperatures than SuperPower and SuperOx conductors. The bonding of SuNAM conductors is not directly comparable to the others due to the isolation of the REBCO surfaces by the Cu oxide surface coat, and will therefore be excluded from this portion of the discussion. Qualitatively correlating the homogeneity of the bonded interface for the different conductors with the surface roughness values in Table 1, it is tempting to claim that film smoothness may be responsible for this disparity. Yet, if only a critical RMS roughness is required, the smooth films on wafers should also have bonded at 600 ^{o}C. Rather, the distinction appears to originate from the effectiveness of pressure-assisted sintering applied to AMSC as opposed to SuperPower and SuperOx.

Pressure-assisted sintering occurs when microscopic features such as pores locally amplify the macroscopic stress applied to the system. Pressure assistance was required to bond AMSC conductors at 600 ^{o}C, but the effect did not extend to SuperPower and SuperOx conductors. This identifies microstructural differences, not smoothness, as responsible for the difference in bonding temperature. AMSC's morphology is characterized by small round features arranged in gradual slopes, not unlike a desert landscape. In contrast, SuperPower and SuperOx surfaces are characterized by relatively flat films with large particles irregularly spaced across the surface. In the case of interfaces, pores are created by frequent but disconnected points of contact between the two surfaces, similar to the way particles contact each other in a green pressed pellet. If each surface feature provides one possible point of contact (at its highest point from the film surface), then it becomes clear that small, densely packed features provide significantly more interfacial points of contact and therefore pores than large features that are less densely located. A fine-featured surface then, such as AMSC's, not only enables pressure assistance in sintering, but also provides improved degrees of contact between surfaces. In fact, in the case of smooth surfaces with effectively no features, contact can be easily foiled by imperfections in the processing atmosphere such as dust.

Evaluation of AMSC joints

Assessing the merits of this approach to superconducting joints requires more context than a simple statement of critical parameters. At face value, the parameters reported above are significantly depressed as compared to the parent conductor, but there are several reasons for this, some of which are related to the bonding process and some which are not. To begin, there are a couple of possible contributions for the several orders-of-magnitude reduction in I_c. First, the lap joint nature of the bond requires that the current at least briefly travel along the c-direction in the REBCO crystal structure. The anisotropy of REBCO's properties are well established; in fact, the anisotropy factor was recently measured to be 500-600, decreasing the critical current density (J_c) from 2.2 MA/cm^2 to 4 kA/cm^2 at 77 K[7]. Without J_c values for the joints discussed here, it is difficult to assess the quality of the interface with respect to current carrying capacity. Although area values can be estimated from joints imaged after testing, visual measurement does not account for portions of the joint which either break during cooling or are isolated due to cracks. From an engineering perspective, a more useful figure of merit could be defined as the ratio of joint I_c to the a-b plane parent I_c, indicating fractional I_c retained; however, this parameter does not account for the effect of mechanical degradation of the film in the joint region. These cracks may reduce the current-carrying capacity of the parent film, restricting the current which actually reaches the bonded region.

The other critical parameter reduced during the joining process is T_c. Commonly, T_c reduction indicates a reduced oxygen stoichiometry; yet the low temperatures and O_2 atmosphere this process utilizes should prevent oxygen loss. YBCO thin film stability studies state that the conductors should not have undergone the orthorhombic/tetragonal transition which accompanies O_2 loss under these conditions, and the process remains well below either the decomposition or peritectic temperatures of the system[5,8]. Furthermore, the bulk retention of T_c as measured by SQUID and resistance measurements imply the source of T_c depression is relegated to a thin interfacial layer. The transverse PPMS measurements of the AMSC joints in Figure 3 support this idea; the first resistance drop corresponds to the bulk T_c of 90 K, whereas the second demonstrates that the conductor had been damaged somewhere else along the current path. Neither SQUID nor PPMS allow for further probing of the possibility of conductor with spatially relegated chemical changes. The origin of the depressed transition is ultimately diagnosed by the ToF-SIMS ionic depth profiles. The ion distributions depicted in Figure 7 highlight two potential causes of low T_c: Ni in the first few nanometers of the film, and an oxygen content which decreases across the film. Ni is commonly said to "poison" REBCO; specifically, it dissolves into the structure and occupies some of the Cu sites, which is correlated with depressions of T_c down to 60 K depending on concentration[9]. While this effect should not be ignored, the observed T_c of 68 K requires that Ni occupy 8.2% of the Cu sites or 2% of a YBCO film; the XPS results confirm that the surface concentration is below 0.1%[9]. Given the insufficiency of the Ni concentration as the main source of T_c depression, the decreasing O content uncovered in SIMS is revealed as the main culprit. Assuming the REBCO near the substrate remains at full oxygen stoichiometry ($x = 0$) and the low content at the surface limits the T_c (corresponding to $x = 0.29$), a linear variation would allow ~620 nm of REBCO to retained full T_c[10]. This agrees well with the in-plane resistivity measurements, which indicate the availability of an in-plane current path with 90 K T_c.

V. CONCLUSIONS

Solid state bonding is a promising approach to joining REBCO CCs while minimizing the O loss that accompanies higher temperature processes. Comparing the results of this technique between

conductors from four manufacturers reveals the importance of phase pure surfaces and the preference for the morphology of AMSC conductors. Only bonds between AMSC conductors display fully homogeneous interfaces with retained superconducting properties. The bonded AMSC conductors carry an I_c in the range of 0.5-20 A with a reduced T_c of ~68 K. Several factors contribute to the I_c reduction, including forced c-axis transport and cracking which occurs during bonding. The T_c depression originates from an oxygen content which decreases linearly from the film substrate to its surface.

ACKNOWLEDGEMENTS

This work partially supported by the U.S. Department of Energy through the Office of Science, Office of High Energy Physics under contract PO 614877. This work was performed in part at the Analytical Instrumentation Facility (AIF) at North Carolina State University, which is supported by the State of North Carolina and the National Science Foundation (award number ECCS-1542015). The AIF is a member of the North Carolina Research Triangle Nanotechnology Network (RTNN), a site in the National Nanotechnology Coordinated Infrastructure (NNCI).

List of Tables and Figures

Table 1: RMS roughness values for all four manufacturer's conductors as well as the wafer grown REBCO samples, as measured by atomic force microscopy.

Manufacturer	Roughness (nm)
AMSC	24.3
SuNAM	90.6
SuperPower	91.5
SuperOx	61.5
Theva	6 - 10

Figure 1: Device used to apply pressure and/or electric field to REBCO conductors during bonding.

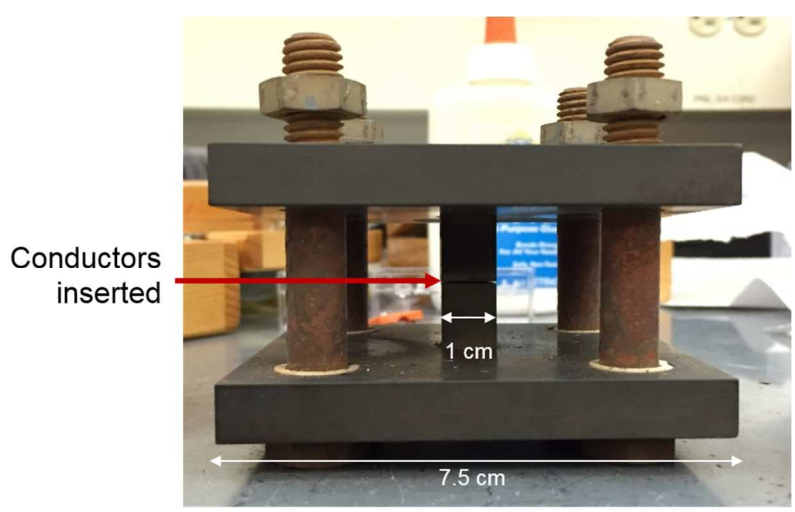

Figure 2: Surface images of conductors before bonding and cross-sections of bonded conductors for SuNAM (a,b), SuperOx (c,d), SuperPower (e,f), and AMSC (g,h) conductors.

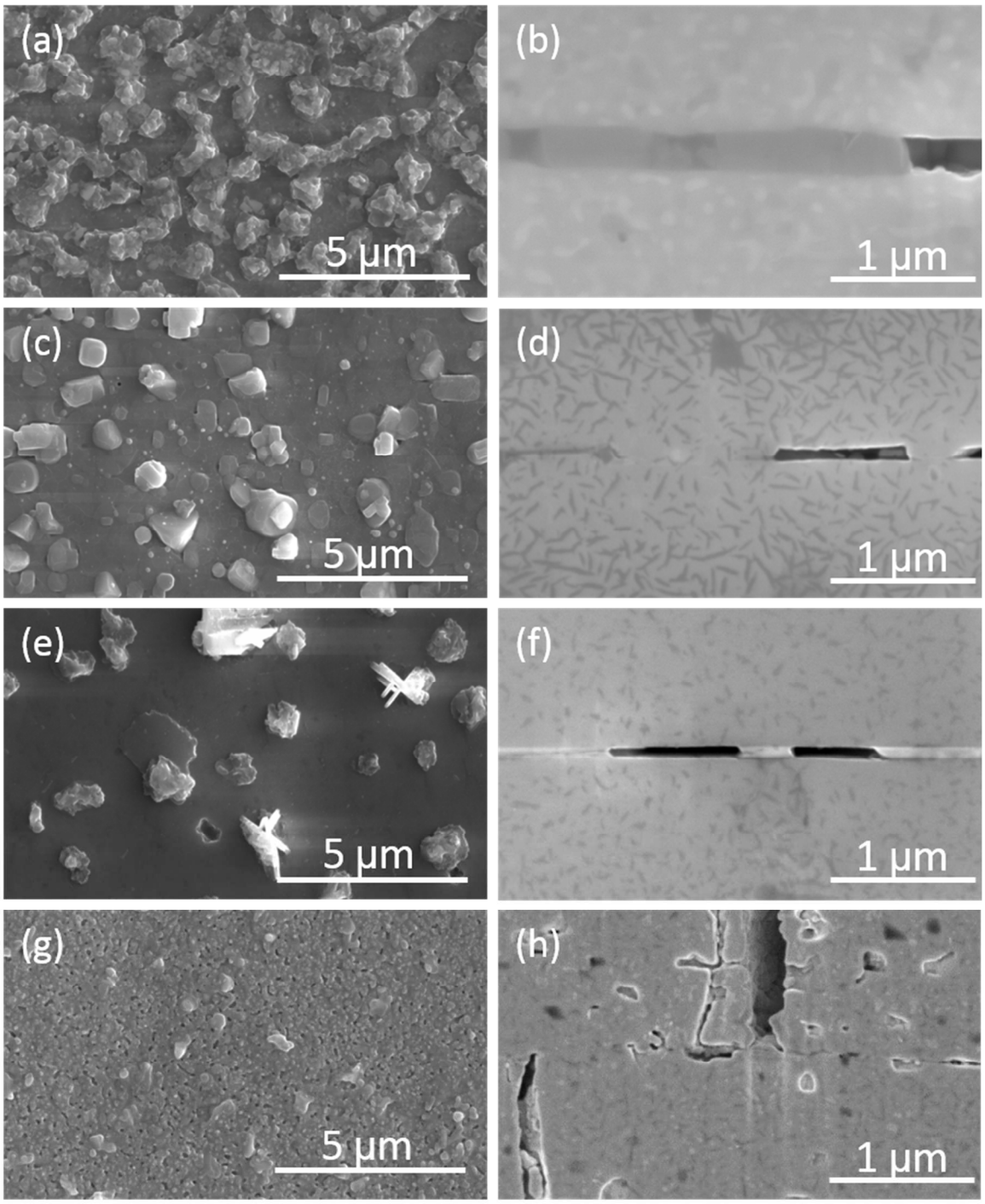

Figure 3: Resistance versus temperature for joints between conductors from each manufacturer. The dotted line indicates the sensitivity limit of the PPMS used for the measurements.

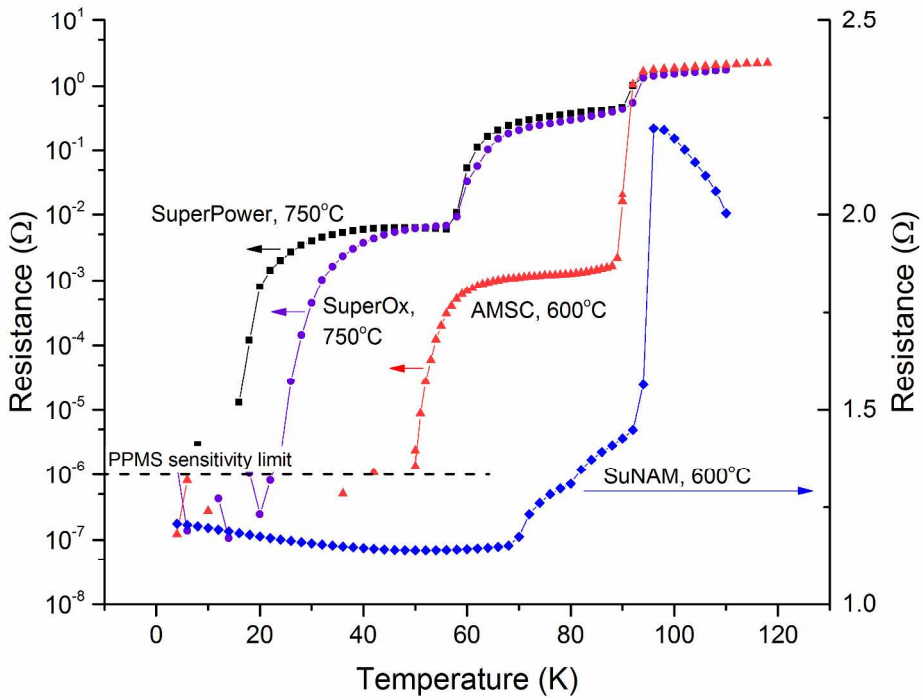

Figure 4: EDS maps of an AMSC joint processed at 600 °C and 3 V.

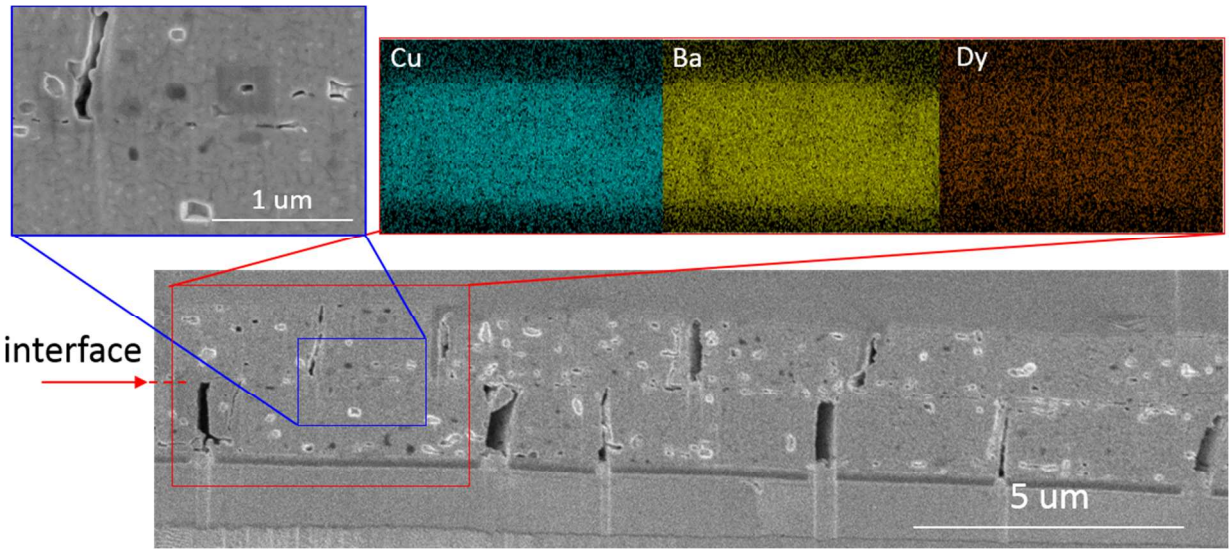

Figure 5: I_c normalized by I_{cmax} vs. temperature for AMSC joints processed at 600 °C with and without electric field, and at 750 °C without electric field.

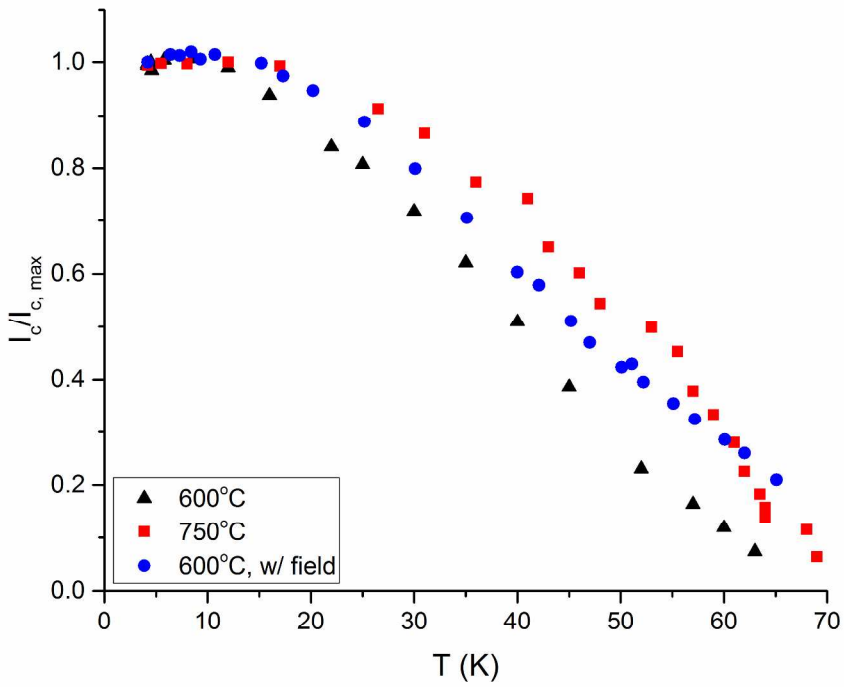

Figure 6: (a) Magnetization versus temperature for a SuperPower conductor after joining and (b) resistance versus temperature for a single AMSC conductor after a heat treatment mimicking the joining process. The inset graph in (b) depicts the same data in log form to show the abrupt disappearance of resistance at 90 K, contrary to the data shown in Figure 3.

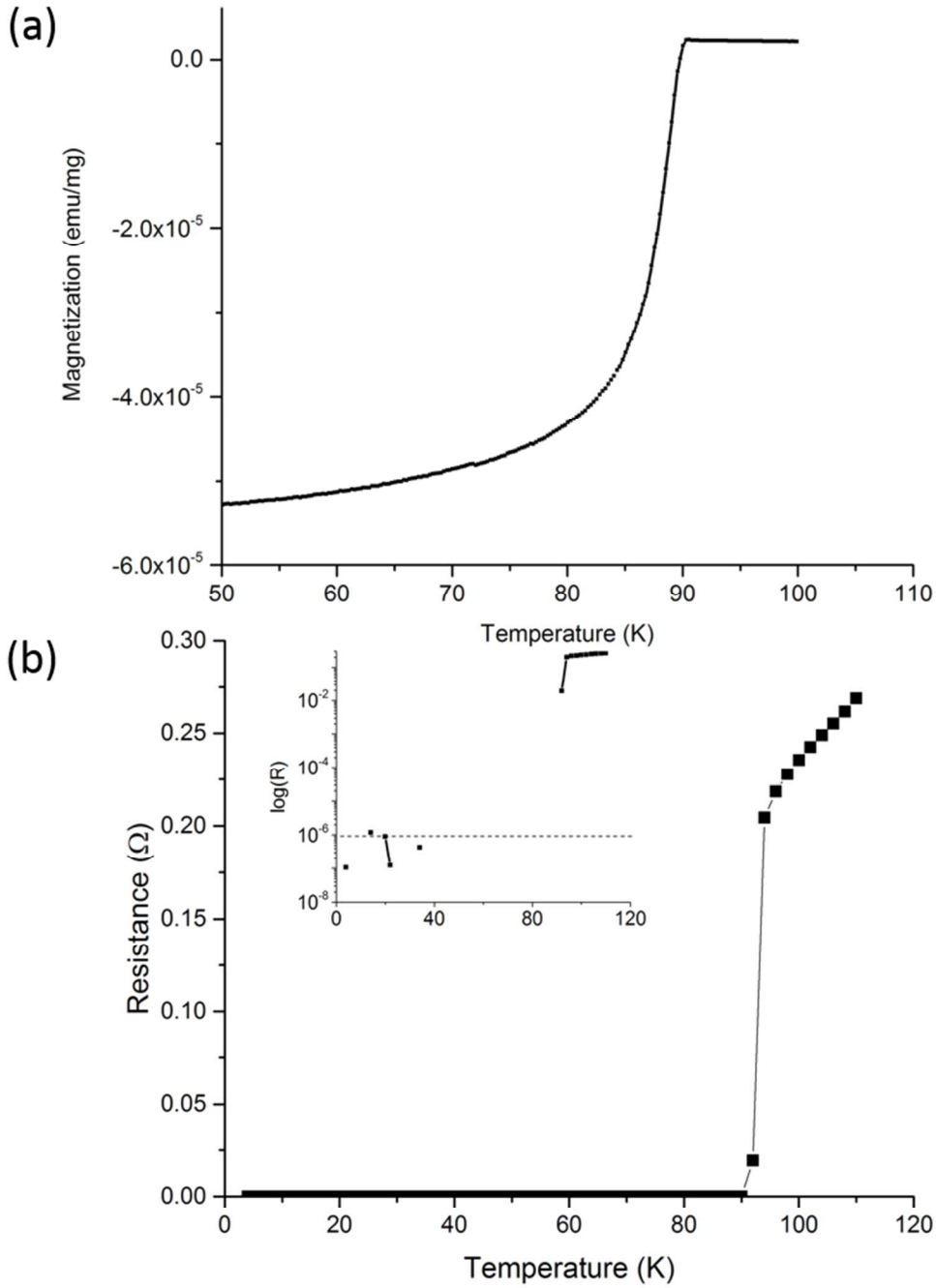

Figure 7: TOF-SIMS depth profiles of (a) Ni and (b) O ions for AMSC REBCO layers with the Ag cap intact, after etching, and after etching and quench annealing to 600 ^{o}C.

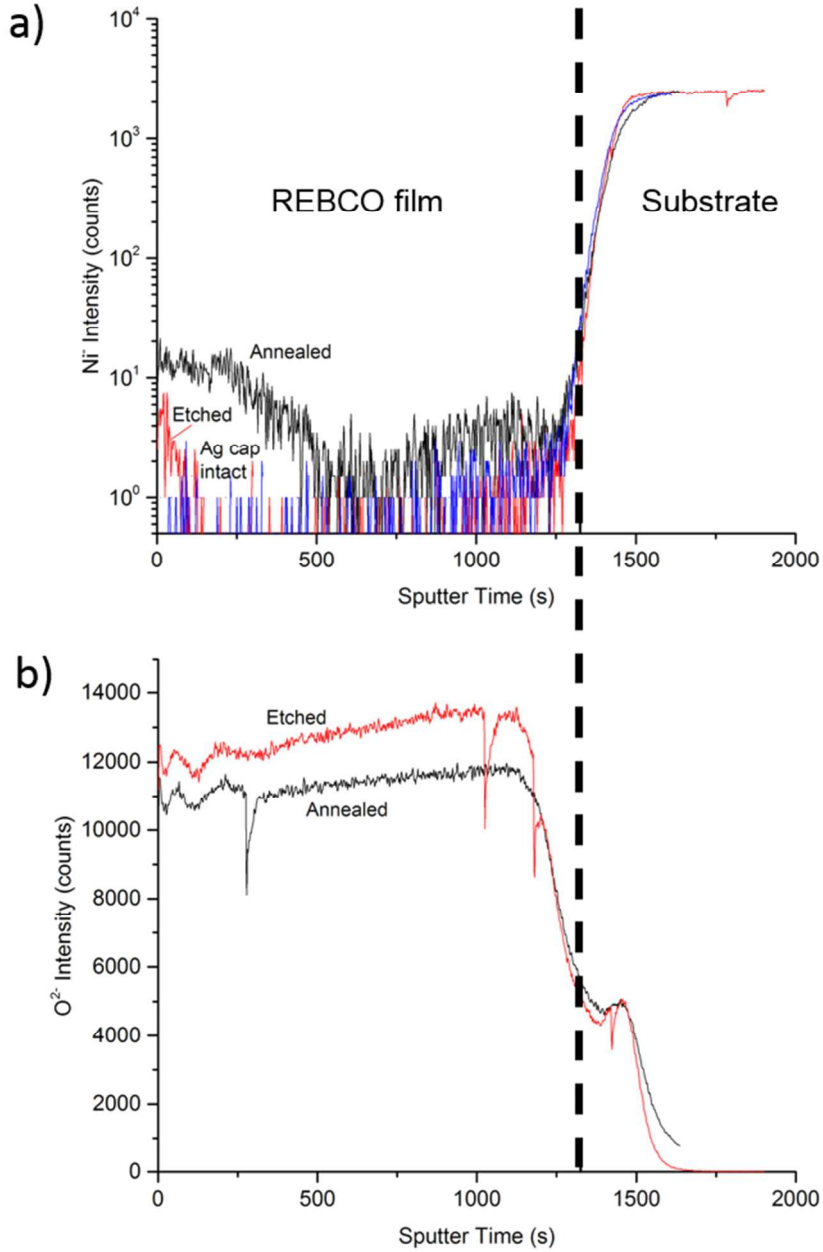

References

[1] Tsui Yeekin, Surrey Elizabeth, and Hampshire Damian, Superconductor Science and Technology **29** (7), 075005 (2016); Shin Hyung-Seop, Kim Jong-min, and J. Dedicatoria Marlon, Superconductor Science and Technology **29** (1), 015005 (2016); J. Y. Kato, N. Sakai, S. Tajima, S. Miyata, M. Konishi, Y. Yamada, N. Chikumoto, K. Nakao, T. Izumi, and Y. Shiohara, Physica C-Superconductivity and Its Applications **445**, 686 (2006).

[2] T. Mousavi G.D. Brittles, C.R.M. Grovenor, C. Aksoy, S.C. Speller, Superconductor Science and Technology **28**, 24 (2015).

[3] Y. Park, M. Lee, H. Ann, Y. H. Choi, and H. Lee, Npg Asia Materials **6**, 5 (2014).

[4] T. Prikhna, W. Gawalek, V. Moshchil, A. Surzhenko, A. Kordyuk, D. Litzkendorf, S. Dub, V. Melnikov, A. Plyushchay, N. Sergienko, A. Koval, S. Bokoch, and T. Habisreuther, Physica C **354** (1-4), 333 (2001); D. A. Cardwell, A. D. Bradley, N. H. Babu, M. Kambara, and W. Lo, Supercond. Sci. Technol. **15** (5), 639 (2002); L. H. Chen, H. Claus, A. P. Paulikas, H. Zheng, and B. W. Veal, Supercond. Sci. Technol. **15** (5), 672 (2002).

[5] R. Cloots, T. Koutzarova, J. P. Mathieu, and M. Ausloos, Superconductor Science and Technology **18** (3), R9 (2005).

[6] Randall M. German, *Sintering Theory and Practice*. (John Wiley & Sons, Inc., New York, NY, 1996).

[7] Y. Jia, J. Hua, G. W. Crabtree, W. K. Kwok, U. Welp, A. P. Malozemoff, M. Rupich, and S. Fleshler, Superconductor Science and Technology **23** (11), 115017 (2010).

[8] J. S. Kim and D. R. Gaskell, Journal of the American Ceramic Society **77** (3), 753 (1994).

[9] Youwen Xu, R. L. Sabatini, A. R. Moodenbaugh, Yimei Zhu, S. G. Shyu, M. Suenaga, K. W. Dennis, and R. W. McCallum, Physica C: Superconductivity **169** (3), 205 (1990).

[10] Jinhua Ye and Keikichi Nakamura, Physical Review B **48** (10), 7554 (1993).